Journal of Innovative Optical Health Sciences
Vol. 9, No. 2 (2016) 1650004 (8 pages)

DOI: 10.1142/S1793545816500048

World Scientific
www.worldscientific.com

Au-nanocluster-loaded human serum albumin nanoparticles with enhanced cellular uptake for fluorescent imaging

Boris Khlebtsov[*,†,‡], Artur Prilepskii[*], Maria Lomova[†] and Nikolai Khlebtsov[*,†]

[*]*Institute of Biochemistry and Physiology of Plants and Microorganisms Russian Academy of Sciences 13 Prospekt Entuziastov Saratov 410049, Russia*

[†]*Saratov State University 83 Ulitsa Astrakhanskaya, Saratov 410012, Russia*

[‡]*bkhl@ibppm.sgu.ru*

Received 20 April 2015
Accepted 24 June 2015
Published 12 August 2015

Protein-directed fluorescent Au nanoclusters have been widely studied owing to their potential applications in sensing, imaging, and drug and gene delivery. However, the use of nanoclusters in drug delivery is limited by low cellular uptake. In this study, human serum albumin-directed Au nanoclusters served as building blocks to obtain protein nanoparticles by desolvation. The nanoparticles had a decent quantum yield (QY), high colloidal stability and low cytotoxicity, and they could be readily conjugated with biological molecules. The cellular uptake of the Au nanoclusters and nanocluster-loaded protein nanoparticles were studied by confocal fluorescence microscopy. Agglomeration of the protein-directed Au nanoclusters into 50–150-nm nanoparticles dramatically increased the cellular uptake.

Keywords: Au nanoclusters; albumin nanoparticles; uptake; fluorescence.

1. Introduction

Au nanoclusters (AuNCs) are a new type of luminescent nanomaterials, typically composed of a few to about a hundred Au atoms.[1] With the cluster dimensions approaching the Fermi wavelength of electrons, the continuous density of states breaks up into discrete energy levels, leading to strong photoluminescence with a large Stokes shift.[2] Compared with other types of luminescent materials, AuNCs have many advantages, among which are good water solubility, low toxicity, biocompatibility, and surface functionalization.[3] Water-soluble

‡Corresponding author.

luminescent AuNCs of high quality and uniformity have been synthesized by various approaches, including microwave-assisted,[4,5] etching-based,[6–8] kinetically controlled[9] and template-directed[10–12] synthesis. Most of these approaches consist in mildly reducing Au ions in the presence of thiol-containing stabilizers. The use of serum proteins, e.g., bovine serum albumin (BSA) and human serum albumin (HSA), as biocompatible reducing and stabilizing agents gives rise to AuNCs with strong red emission and a decent QY,[13,14] comparable to that of upconverting[15] or dye-doped[16] nanoparticles. Owing to their easy synthesis, biocompatibility, and excellent fluorescent properties, AuNCs have been useful in various applications, including sensing[17–19] and bioimaging *in vitro* and *in vivo*.[20–22] Yet, there have been only a few studies dealing with the application of AuNCs in fluorescence (FL)-guided drug delivery. For example, Chen *et al.*[23] used folic-acid-conjugated Au–BSA NCs for the delivery of doxorubicin (DOX) into tumors. An important limiting factor, however, is the low cellular uptake of AuNCs owing to their being only a few nanometers in size. On the other hand, albumin nanoparticles are well known as biodegradable carriers for the delivery of anticancer drugs because of their excellent biocompatibility, stability in blood, and high cellular uptake.[24,25] They can be easily fabricated by the desolvation[26] or water-in-oil (w/o) emulsion method,[27] followed by cross-linking with glutaraldehyde or heating. HSA nanoparticles have been utilized in controlled release studies owing to the enhanced permeability and retention effects, which lead to accumulation of particles of certain size at tumor sites.[28–32]

In this paper, we propose the use of HSA-directed AuNCs as building blocks for fluorescent HSA nanoparticles. We show that after desolvation and crosslinking, the Au–HSA NCs retain their FL properties. We show further that the NC-loaded nanoparticles with sizes of 50–150 nm exhibit low cytotoxicity and higher cellular uptake in comparison with the initial NCs.

2. Materials and Methods

2.1. *Reagents*

All chemicals were obtained from commercial suppliers and were used without further purification. Hydrogen tetrachloroaurate(III) hydrate ($HAuCl_4$), BSA, and HSA were obtained from Sigma-Aldrich. Hydrogen tetrachloroaurate trihydrate ($HAuCl_4 \cdot 3H_2O$) was purchased from Alfa Aesar. Ultrapure water obtained from a Milli-Q Integral 5 system was used in all experiments.

2.2. *Synthesis of Au–HSA NCs and nanoparticles*

Au–HSA NCs were prepared by protein-directed synthesis at high temperature and pH.[13] In a typical procedure, 5 mL of 4.8 mM $HAuCl_4$ was added to 5 mL of HSA solution (20 mg/mL) under vigorous magnetic stirring for 2 min. Then, 20 mL of 1 M NaOH was introduced to adjust the pH to 10. The mixture was heated in an oil bath at 100°C for 30 min under vigorous magnetic stirring. During this period, the solution color changed from light-yellow to brown, indicating the formation of small AuNCs inside the protein matrix. After the solution had been cooled to room temperature, the product was collected with an Amicon Ultra-15 centrifuge concentrator (MW cutoff, 10,000) and was redispersed in 10 mL of water. The final HSA concentration was 10 mg/mL. For cell experiments, the NCs were redispersed in 100 mL of phosphate-buffered saline (PBS; 100 mM, pH 7.4) to a final protein concentration of 1 mg/mL.

AuNC-loaded HSA nanoparticles were prepared by simple desolvation. To this end, 2 mL of as-prepared Au–HSA NCs (10 mg/mL, pH 10), put in a 30°C thermostatic bath, was mixed with 100 μL of 1 M NaCl, after which 7 mL of absolute ethanol was added with a syringe pump at 5 mL/min. The solution became turbid, and after 5 min, 30 μL of 25% glutaraldehyde was added as the crosslinking agent. The mixture was left under continuous stirring for 8 h. The sample was purified by three cycles of centrifugation at 14,000 rpm for 30 min and was redispersed in a glycine buffer. The nanoparticles were incubated in an amino-acid-containing buffer for 4 h to totally eliminate the glutaraldehyde groups on the surface. Finally, the Au–HSA nanoparticles were collected with an Amicon Ultra-15 centrifuge concentrator (MW cutoff, 10,000) and were redispersed in PBS (100 mM, pH 7.4) to a final protein concentration of 1 mg/mL.

2.3. *Characterization*

FL spectra were recorded with an LS-55 FL spectrophotometer (Perkin Elmer). Transmission electron microscopy (TEM) images were taken with a Libra-120 microscope (Carl Zeiss) at the Simbioz Center for the Collective Use (CCU) of Research Equipment in the Field of Physical–Chemical Biology and Nanobiotechnology at the Russian Academy of Sciences' Institute of Biochemistry and Physiology of Plants and Microorganisms (IBPPM RAS). The hydrodynamic radius of the nanoparticles was measured with a Malvern ZS dynamic light scattering device. Images of the samples under UV irradiation were captured with a Canon digital camera and a Vilber Lourmart transilluminator (365 nm, Sigma–Aldrich).

2.4. *Cell cultures*

The SPEV and A549 lung cancer cell lines were obtained from the Saratov Science Research Veterinary Station, Saratov, Russia. The cells were cultured in RPMI-1640 growth medium containing 10% fetal bovine serum and 1% antibiotics (gentamicin and amphotericin) at 37°C and 5% CO_2 for 7 days until a concentration of $(5 \text{ to } 8) \times 10^8$ cells/cm^3 was reached.

Cell metabolic activity was measured by the MTT (3-[4, 5-dimethylthiazol-2-yl]-2, 5 diphenyl tetrazolium bromide) assay. In brief, after incubation with AuNCs or with NC-loaded nanoparticles, the cells were incubated in 0.5 mL of an MTT solution (Sigma, USA) for 1 h. Then, the cells were redispersed in 0.5 mL of dimethyl sulfoxide (ACS grade, Amresco, USA) to dissolve the formazan crystals. The samples were centrifuged at 12,000 g for 5 min in 1.5-mL eppendorf tubes, and 0.2 mL of the supernatant liquid was transferred to 96-well plates. Absorbance values at 492 nm were collected on a Multiskan Ascent microplate reader (Thermo Fisher Scientific).

Cellular uptake was estimated by incubating the SPEV cells with Au–HSA NCs and nanoparticles (HSA concentration, 50 μg/mL) in RPMI-1640 medium in 24-well plates. After 2 h incubation, the cells were washed with 100 mM PBS (pH 7.4). Differential inference contrast and confocal FL images were obtained with a Leica SP7 microscope (illumination, 514 nm; FL accumulation channel, 600–700 nm; objective, $\times 10$).

3. Results and Discussion

3.1. *Synthesis and characterization of NCs and nanoparticles*

First, Au–HSA NCs were prepared from a boiling mixture of HSA and Au_3^+ under highly basic conditions. According to Ulbrich *et al.*,[29] Au–HSA NCs are composed of 20 (Ref. 14) or 25 (Ref. 29) Au atoms and are stabilized by the thiol group of cysteine.

Figure 1(a) shows the excitation and emission spectra of the Au–HSA NCs. The FL excitation

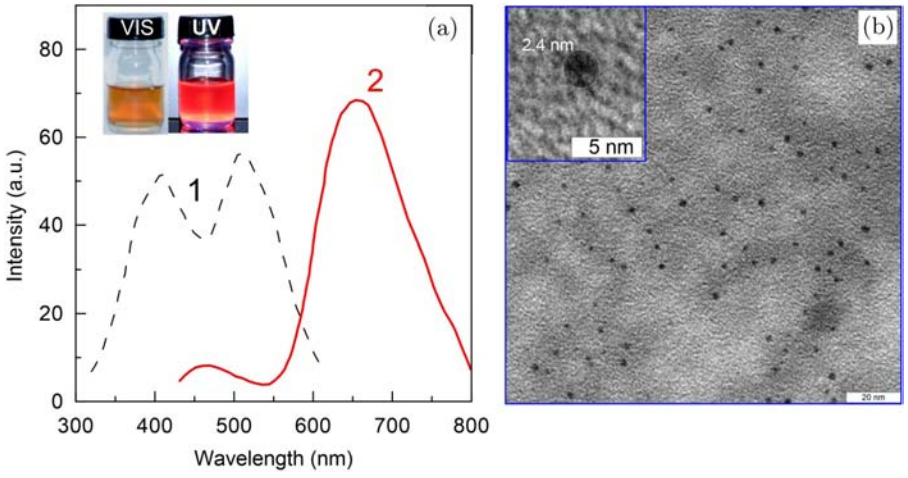

Fig. 1. (a) Excitation (1) and emission (2) spectra of the Au–HSA NCs. (b) TEM images of the Au–HSA NCs. The inset in panel (a) shows photos of NC solutions under white light (left) and UV light (right) irradiation. The inset in panel (b) shows a magnified image of a single NC.

spectrum (curve 1) exhibits two maxima around 410 nm and 504 nm. The emission peaks are located near 470 nm and 660 nm. The first peak could be due to the FL of albumin alone, whereas the second peak may have originated from AuNCs inside the protein matrix. Under optimal conditions, the QY of the NCs was about 10.4%, as measured with hematoporphyrin as a benchmark standard. This value is in harmony with the earlier established correlation between the NC sizes and their QYs[32] for Au_{25}NCs.

As shown in the inset of Fig. 1(a), the as-prepared Au–HSA NCs were highly dispersed in aqueous solution and exhibited a brown color under white light and strong red FL under UV illumination. In general, the absence of a reddish color under vis illumination indicates the formation of only small (< 3 nm) AuNCs which have no plasmonic peak around 510–520 nm. The TEM images of the NCs [Fig. 1(b)] also confirm the absence of large or aggregated nanoparticles, and the average size of the Au–HSA NCs was about 2.4 nm, close to the previously reported values for Au_{20}[13] and Au_{25}[33] NCs.

Since the protein content of the Au–HSA NCs was more than 96% (100 mg of HSA and 4 mg of Au in one batch), we used a well-known desolvation protocol to prepare NC-loaded nanoparticles.[26] To this end, ethanol was added dropwise to an aqueous Au–HSA solution under constant stirring at the desired temperature and concentration. As HSA is less soluble in alcohol, the albumin molecules aggregated into nanoparticles when the concentration of ethanol became higher than 70%. During desolvation, the color of the sample changed from light yellow to milky white [see left inset in Fig. 2(a)]. For keeping the nanoparticle morphology constant, the protein was further crosslinked by glutaraldehyde.

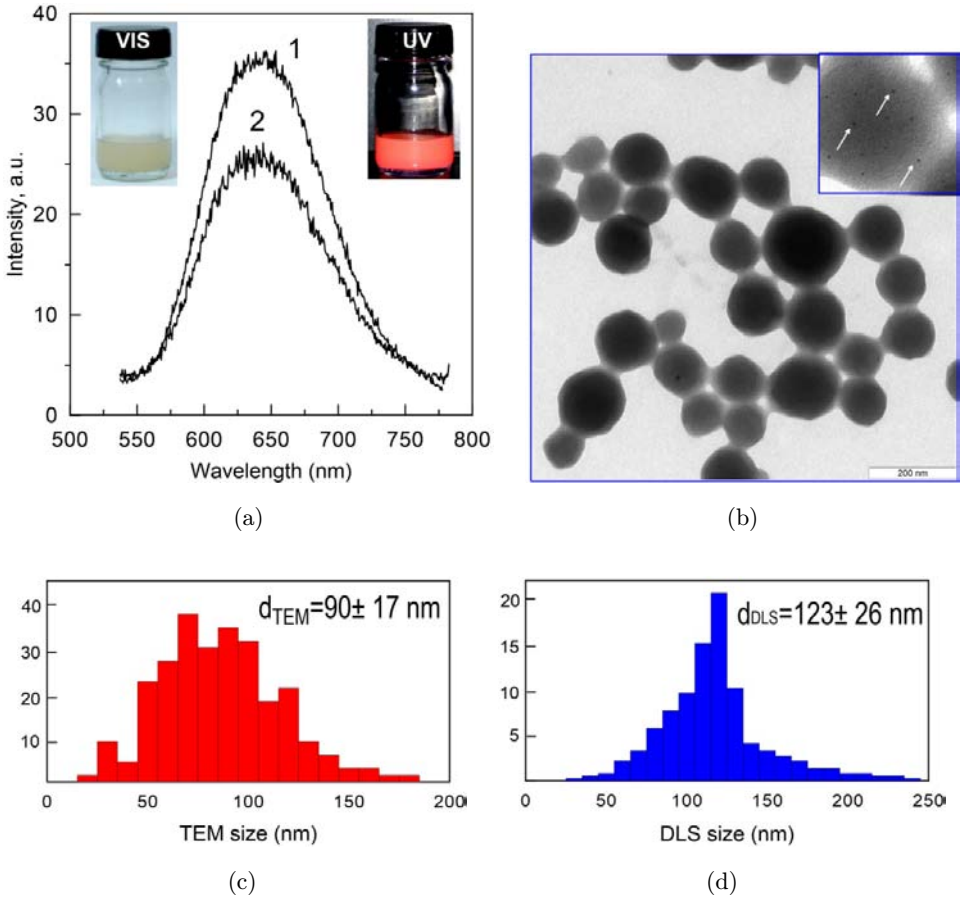

Fig. 2. (a) FL spectra of diluted (1:100) Au–HSA NCs (curve 1) and NC-loaded nanoparticles (curve 2). The insets show images of nanoparticle suspensions under vis (left) and UV (right) illumination. (b) TEM image of the nanoparticles. The inset shows a magnified image of a single nanoparticle. The arrows indicate the position of the Au–HSA NCs in the protein nanoparticles. (c) Histogram of the nanoparticle size distribution obtained by TEM measurements. (d) Histogram of the nanoparticle size distribution obtained by dynamic light scattering (DLS) measurements.

The influence of critical parameters of synthesis such as pH, temperature, ionic strength, rate of addition of the desolvating agent, and amount of agent added on the final albumin nanoparticle size and polydispersity have been studied previously.[34,35] In this work, we used optimized parameters, which led to the formation of nanoparticles with a size of about 100 nm and a yield of 98%.

Figure 2(b) shows a TEM image of as-prepared nanoparticles made of Au–HSA NCs as building blocks. Statistical TEM analysis indicated that the nanoparticles had a spherical shape and a size distribution of 50 nm to 150 nm [Fig. 2(c)]. The average size obtained by TEM was 90 nm, whereas DLS measurements of the hydrodynamic size gave a value of 120 nm [Fig. 2(d)]. This difference between TEM and DLS results is commonly observed and has already been discussed previously.[36] The presence of small AuNCs inside the polymer nanoparticles cannot be resolved at moderate TEM magnifications [Fig. 2(b)], but they can be identified in the enlarged and contrasted TEM image shown in the inset. The successful inclusion of the AuNCs became clear once the sample was observed under vis and UV illumination. The nanoparticle suspension looked milky white under vis illumination, and strong red FL appeared under UV illumination [see insets in Fig. 2(a)]. It is well known that aggregation of organic dyes and semiconductor quantum dots results in quenching of FL. To estimate the influence of NC aggregation into nanoparticles on FL QY, we compared the spectra of the Au–HSA NCs and nanoparticles with the same concentration [Fig. 2(a)]. Note that the spectra were measured for diluted samples with a protein concentration of 0.01 mg/mL and an absorbance at 400 nm of about 0.01. The samples were diluted 100-fold to exclude the inner filter effect for the turbid nanoparticle sample.[37] The FL spectra of the AuNC-loaded nanoparticles had the same maximum wavelength and full width at half maximum as the Au–HSA NCs. On the other hand, we observed a 25% decrease in FL intensity during self-assembly into nanoparticles. We believe that a key role in the loss of FL intensity could be played by the scattering of incident and emitted light by the protein, since this effect disappears in the case of single particle illumination, e.g., during confocal FL microscopy. In general, we can conclude that AuNCs retain their fluorescent properties during self-assembly into nanoparticles.

3.2. *Cytotoxicity and cellular uptake*

For proving the potential utility of AuNC-loaded nanoparticles as a new agent for cellular imaging and drug delivery, we examined the viability of A549 and SPEV cells (MTT assay, see Sec. 2) at various concentrations of Au–HSA NCs and nanoparticles (Fig. 3). In good agreement with the published data for different types of AuNC,[38–40] the viability of the SPEV cells was not affected by

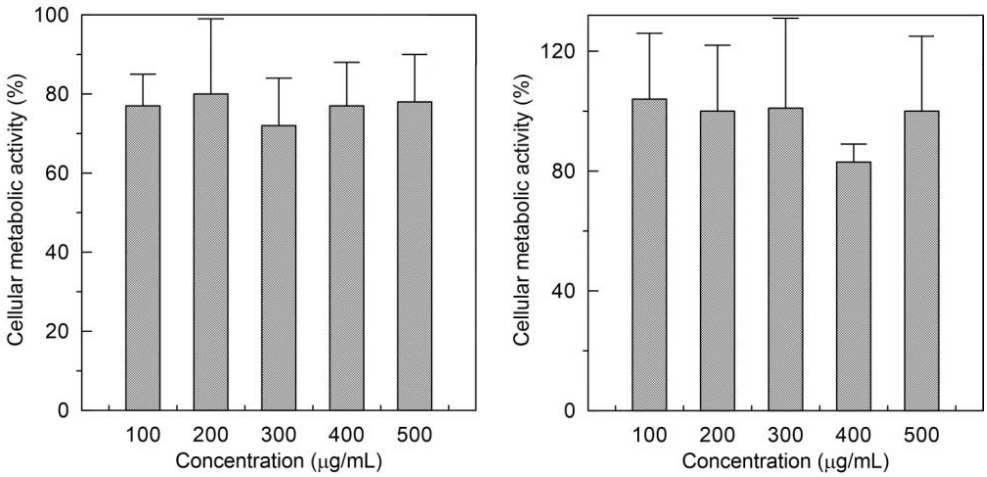

Fig. 3. Viability of the SPEV (a,b) and A549 (c,d) cells after exposure to different concentrations of NC-loaded protein nanoparticles (a,c) and Au–HSA NCs (b,d). Viability was determined by the MTT assay. The error bar represents the standard error of eight trials.

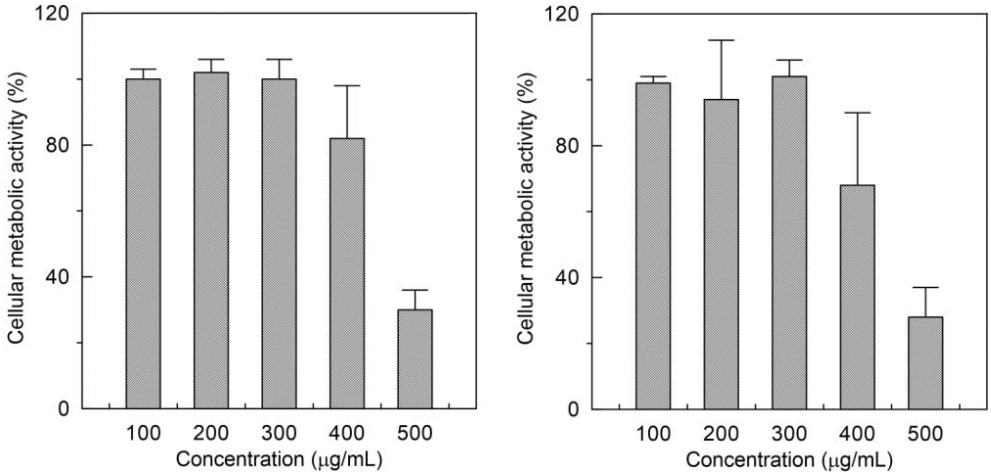

(c) (d)

Fig. 3. (*Continued*)

co-incubation with 100–500 μg/mL Au–HSA for 24 h [Fig. 3(b)], whereas the A459 lung cancer cells exhibited a decreased metabolic activity only when incubated with relatively high concentrations of the nanomaterial.

The same result was obtained for the NC-loaded protein nanoparticles. These two types of biomaterials were further employed as optical probes for passive targeting imaging of cancer cells *in vitro*.

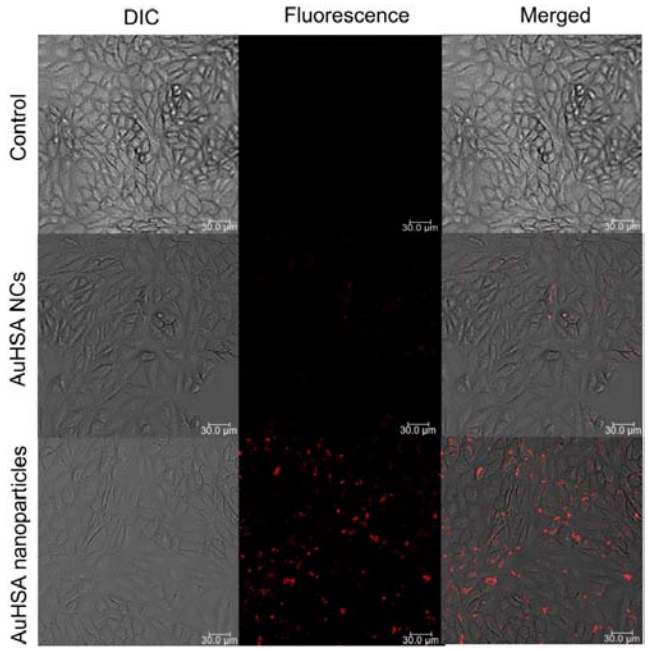

Fig. 4. Delivery of Au–HSA NCs and NC-loaded HSA nanoparticles into live SPEV cells. Differential interference contrast (DIC), FL, and an overlay of these modes are given. Scale bars are 30 μm.

The SPEV cells showed strong red FL after incubation with NC-loaded HSA nanoparticles for 2 h and very weak FL after incubation with pure Au–HSA NCs (Fig. 4). The weak penetration of the NCs into the live cells confirmed the limitation on the uptake of very small (< 5 nm) Au nanoparticles and protein molecules via endocytosis (i.e., passive targeting). To be sure that the NC-loaded nanoparticles penetrated the cells rather than simply being adsorbed on the surface, we performed z-stack scanning of the cells. The successive images made in the different z-stacks from substrate plate to cell top (https://www.youtube.com/watch?v=GAGrtA-WfFM&feature=youtu.be) clearly demonstrate that most of the nanoparticles were present inside the cells.

4. Conclusions

HSA-directed AuNCs have been used as building blocks to obtain protein nanoparticles. The nanoparticles have a spherical shape and a size of about 100 nm, and they retain the fluorescent properties of the initial AuNCs. The cellular uptake of the Au–HSA NCs and NC-loaded HSA nanoparticles has been studied by confocal FL microscopy to prove that NC-loaded HSA nanoparticles have potential as a new agent for cellular imaging and drug delivery. We have found that the aggregation of albumin molecules into nanoparticles improves their uptake into cancer cells. This finding can have an important role to play in the use of protein-based

fluorescent nanomaterials as drug delivery platforms.

Acknowledgments

This work was supported by the Russian Scientific Foundation (project no. 14-13-01167). The work by B.N.K. (AuNC synthesis) was partly supported by a grant from the Russian Foundation for Basic Research (no. 15-33-20248).

References

1. M. Cui, Y. Zhao, Q. Song, "Synthesis, optical properties and applications of ultra-small luminescent gold nanoclusters," *Trends Anal. Chem.* **57**, 73 (2014).
2. J. Zheng, C. Zhang, R. M. Dickson, "Highly fluorescent, water-soluble, size-tunable gold quantum dots," *Phys. Rev. Lett.* **93**, 077402 (2004).
3. L. Shang, S. J. Dong, G. U. Nienhaus, "Ultra-small fluorescent metal nanoclusters: Synthesis and biological applications," *Nano Today* **6**, 401 (2001).
4. L. Yan, Y. Q. Cai, B. Z. Zheng, H. Y. Yuan, Y. Guo, D. Xiao, M. M. F. Choi, "Microwave-assisted synthesis of BSA-stabilized and HSA-protected gold nanoclusters with red emission," *J. Mater. Chem.* **22**, 1000 (2012).
5. Y. Yue, T. Y. Liu, H. W. Li, Z. Y. Liu, Y. Q. Wu, "Microwave-assisted synthesis of BSA-protected small gold nanoclusters and their fluorescence-enhanced sensing of silver(I) ions," *Nanoscale* **4**, 2251 (2012).
6. M. A. H. Muhammed, P. K. Verma, S. K. Pal, A. Retnakumari, M. Koyakutty, S. Nair, T. Pradeep, "Luminescent quantum clusters of gold in bulk by albumin induced core etching of nanoparticles: Metal ion sensing, metal-enhanced luminescence, and biolabeling," *Chem. Eur. J.* **16**, 10103 (2010).
7. M. A. H. Muhammed, P. K. Verma, S. K. Pal, R. C. A. Kumar, S. Paul, R. V. Omkumar, T. Pradeep, "Bright, NIR-emitting Au23 from Au25: Characterization and applications including biolabeling," *Chem. Eur. J.* **15**, 10110 (2009).
8. M. A. H. Muhammed, S. Ramesh, S. S. Sinha, S. K. Pal, T. Pradeep, "Two distinct fluorescent quantum clusters of gold starting from metallic nanoparticles by pH-dependent ligand etching," *Nano Res.* **1**, 333 (2008).
9. M. Z. Zhu, E. Lanni, N. Garg, M. E. Bier, R. C. Jin, "Kinetically controlled, high-yield synthesis of Au25 clusters," *J. Am. Chem. Soc.* **130**, 1138 (2008).
10. Y. F. Kong, J. Chen, F. Gao, R. Brydson, B. J. Johnson, G. Heath, Y. Zhang, L. Wu, D. J. Zhou, "Near-infrared fluorescent ribonuclease-A-encapsulated gold nanoclusters: Preparation, characterization, cancer targeting and imaging," *Nanoscale* **5**, 1009 (2013).
11. X. L. Guevel, N. Daum, M. Schneider, "Synthesis and characterisation of human transferrin-stabilized gold nanoclusters," *Nanotechnology* **22**, 275103 (2011).
12. H. Wei, Z. D. Wang, L. M. Yang, S. L. Tian, C. J. Hou, Y. Lu, "Lysozyme-stabilized gold fluorescent cluster: Synthesis and application as Hg2+ sensor," *Analyst* **135**, 1406 (2010).
13. J. P. Xie, Y. G. Zheng, J. Y. Ying, "Protein-directed synthesis of highly fluorescent gold nanoclusters," *J. Am. Chem. Soc.* **131**, 888 (2009).
14. P. Zhang, X. X. Yang, Y. Wang, N. W. Zhao, Z. H. Xiong, C. Z. Huang, "Rapid synthesis of highly luminescent and stable Au_{20} nanoclusters for active tumor-targeted imaging *in vitro* and *in vivo*," *Nanoscale* **6**, 2261 (2014).
15. C. F. Gainer, M. Romanowski, "A review of synthetic methods for the production of upconverting lanthanide nanoparticles," *J. Innov. Opt. Health Sci.* **7**, 1330007 (2014).
16. J. Zhong, S. Yang, "Contrast-enhanced photoacoustic imaging using indocyanine green-containing nanoparticles," *J. Innov. Opt. Health Sci.* **7**, 1350029 (2014).
17. H. Dai, Y. Shi, Y. Wang, Y. Sun, J. Hu, P. Ni, Z. Li, "Label-free turn-on fluorescent detection of melamine based on the anti-quenching ability of Hg2+ to gold nanoclusters," *Biosens. Bioelectron.* **53**, 76–81 (2014).
18. H.-W. Li, Y. Yue, T.-Y. Liu, D. Li, Y. Wu, "Fluorescence-enhanced sensing mechanism of BSA-protected small gold-nanoclusters to silver(I) ions in aqueous solutions," *J. Phys. Chem. C* **117**, 16159–16165 (2013).
19. B. Aswathy, G. Sony, "Cu2+ modulated BSA-Au nanoclusters: A versatile fluorescence turn-on sensor for dopamine," *Microchem. J.* **116**, 151–156 (2014).
20. S. Choi, R. M. Dickson, J. Yu, "Developing luminescent silver nanodots for biological applications," *Chem. Soc. Rev.* **41**, 1867–1891 (2012).
21. J. Wang, J. Ye, H. Jiang, S. Gao, W. Ge, Y. Chen, C. Liu, C. Amatore, X. Wang, "Simultaneous and multisite tumor rapid-target bioimaging through *in vivo* biosynthesis of fluorescent gold nanoclusters," *RSC Adv.* **4**, 37790–37795 (2014).
22. L.-Y. Chen, C.-W. Wang, Z. Yuan, H.-T. Chang, "Fluorescent gold nanoclusters: Recent advances in sensing and imaging," *Anal. Chem.* **87**, 216–229 (2015).

23. H. Chen, S. Li, B. Li, X. Ren, S. Li, D. M. Mahounga, S. Cui, Y. Gu, S. Achilefu, "Folate-modified gold nanoclusters as near-infrared fluorescent probes for tumor imaging and therapy," *Nanoscale*, **4**, 6050–6064 (2012).
24. L. Xie, T. Weijun, D. Yu, J. Xu, J. Lib, Ch. Gao, "Bovine serum albumin nanoparticles modified with multilayers and aptamers for pH-responsive and targeted anti-cancer drug delivery," *J. Mater. Chem.* **22**, 6053–6060 (2012).
25. Z. Yu, M. Yu, Z. Zhang, G. Hong, Q. Xiong, "Bovine serum albumin nanoparticles as controlled release carrier for local drug delivery to the inner ear," *Nanoscale Res. Lett.* **9**, 343 (2014).
26. C. Weber, C. Coester, J. Kreuter, K. Langer, "Desolvation process and surface characterisation of protein nanoparticles," *Int. J. Pharm.* **194**, 91–102 (2000).
27. M. Trotta, D. Chirio, R. Cavalliand, E. Peira, "Hydrophilic microspheres from water-in-oil emulsions by the water diffusion technique," *Pharm. Res.* **21**, 1445–1449 (2004).
28. A. Jithan, K. Madhavi, M. Madhavi, K. Prabhakar, "Preparation and characterization of albumin nanoparticles encapsulating curcumin intended for the treatment of breast cancer," *Int. J. Pharm. Investig.* **1**, 119–125 (2011).
29. K. Ulbrich, M. Michaelis, F. Rothweiler, T. Knobloch, P. Sithisarn, J. Cinatl, J. Kreuter, "Interaction of folate-conjugated human serum albumin (HSA) nanoparticles with tumor cells," *Int. J. Pharm.* **406**, 128–134 (2011).
30. Y. Liu, Z. Qian, J. Yin, X. Wang, "Tumor therapy by fast moving magnetic nanoparticle under low-frequency alternating magnetic field," *J. Innov. Opt. Health Sci.* **8**, 1550008 (2015).
31. X. Wen, P. Yu, Y.-R. Toh, J. Tang, "Structure-correlated dual fluorescent bands in BSA-protected Au_{25} nanoclusters," *J. Phys. Chem. C* **116**, 11830 (2012).
32. J. Zheng, P. R. Nicovich, R. M. Dickson, "Highly fluorescent noble-metal quantum dots," *Annu. Rev. Phys. Chem.* **58**, 409 (2007).
33. X. L. Guevel, B. Hotzer, G. Jung, K. Hollemeyer, V. Trouillet, M. Schneider, "Formation of fluorescent metal (Au, Ag) nanoclusters capped in bovine serum albumin followed by fluorescence and spectroscopy," *J. Phys. Chem. C* **115**, 10955 (2011).
34. F. Galisteo-González, J. A. Molina-Bolívar, "Systematic study on the preparation of BSA nanoparticles," *Colloids Surf. B Biointerfaces* **123**, 286 (2014).
35. G. Wang, K. Siggers, S. Zhang, H. Jiang, Z. Xu, R. F. Zernicke, J. Matyas, H. Uludağ, "Preparation of BMP-2 containing bovine serum albumin (BSA) nanoparticles stabilized by polymer coating," *Pharm. Res.* **12**, 2896 (2008).
36. B. N. Khlebtsov, V. A. Khanadeev, N. G. Khlebtsov, "Determination of the size, concentration, and refractive index of silica nanoparticles from turbidity spectra," *Langmuir* **24**, 8964 (2008).
37. J. P. Lakowicz, *Principles of Fluorescence Spectroscopy*, 2nd edn., Springer, New York (2004).
38. L. Shang, F. Stockmar, N. Azadfar, G. U. Nienhaus, "Intracellular thermometry by using fluorescent gold nanoclusters," *Angew. Chem. Int. Ed.* **52**, 11154 (2013).
39. Ch. Zhang, Zh. Zhou, Q. Qian, G. Gao, Ch. Li, L. Feng, Q. Wang, D. Cui, "Glutathione-capped fluorescent gold nanoclusters for dual-modal fluorescence/X-ray computed tomography imaging," *J. Mater. Chem. B* **1**, 5045 (2013).
40. P. Bian, J. Zhou, Y. Liu, Zh. Ma, "One-step fabrication of intense red fluorescent gold nanoclusters and their application in cancer cell imaging," *Nanoscale* **5**, 6161 (2013).